

1 **Impact of Hydrostratigraphic Continuity in Heterogeneity on**
2 **Brine-to-Freshwater Interface Dynamics; Implications from a**
3 **2-D Parametric Study in an Arid and Endorheic Basin**

4 **S.V. McKnight^{1*}, D.F. Boutt¹, and L.A. Munk²**

5 ¹Department of Geosciences, 627 North Pleasant Street, 233 Morrill Science Center, University of Massachusetts Amherst,
6 Amherst, Massachusetts 01003

7 ²Department of Geological Sciences, 3211 Providence Drive, University of Alaska Anchorage, Anchorage, Alaska 99508

8 **Key Points:**

- 9 • Increased horizontal continuity of hydrostratigraphic units decreases the slope of brine-
10 to-freshwater interface geometry
- 11 • Increased horizontal hydrostratigraphic continuity increases time required to reach a new
12 dynamic steady state following change in recharge
- 13 • Density-driven flow creates variable interface geometry and sensitivity in heterogeneous
14 media that is not captured in homogeneous media

*Current address

Corresponding author: Sarah McKnight, smcknight@umass.edu

Abstract

Despite the prevalence of density-driven flow systems in brine-rich aquifers of arid climates and coastal aquifers, the impact of realistic geologic conditions remains poorly constrained regarding interface geometry in arid regions and time-sensitive density-dependent dynamics in brine-bearing aquifers in general. Salar de Atacama provides an analog for exploring interface dynamics in arid regions. A site-specific 2D hydrostratigraphic interpretation is used to examine the dynamics of the brine-to-freshwater interface. With the same simulation framework and core data, a separate parametric series of hydraulic conductivity distributions with varying horizontal continuity provides a mechanistic explanation for observed dynamics. Comparing modeled interfaces and their sensitivity to perturbations in recharge in each realization yields insight into interface dynamics coupled with horizontal continuity in subsurface heterogeneity. Recharge fluctuation is introduced to each distribution following the interface reaching a dynamic steady state. Metrics for results evaluation include migration length, interface slope geometry, and response rate. Analyses suggest that the slope of the modeled interface shallows or decreases by 0.01 to 0.05 $\text{m} \cdot \text{m}^{-1}$ for every increase in continuity of highly permeable pathways by a factor. Increasing continuity also increases both the overall response times and the variability in response. Results indicate that accurate representations of transient dynamics in modeling density-driven brine-to-freshwater interface dynamics requires the consideration of heterogeneity, as saline intrusion in the highest continuity group extends over twice as far on average and the modeled interface takes over 43 percent more time on average to reach a new dynamic steady state when compared to their homogeneous counterparts.

Plain Language Summary

Differences in the density of groundwater from dissolved salt causes impacts groundwater flow which behaves differently under different subsurface conditions. This paper focuses on how spatial differences in porosity affects flow behavior and changes the risk of saline groundwater intrusion. Core and groundwater data from the southeastern edge of the salt flat in Salar de Atacama provides information on subsurface physical characteristics and groundwater chemistry. This data is used to create an interpretation of how flow properties vary in time and space. This provides a means for assessing the role of spatially variable geologic units on the geometry and the sensitivity of the brine-to-freshwater interface to changes in recharge to an aquifer. We use distributions of the area's geology to test different amounts of geologic variability in the horizontal versus the vertical direction. Results indicate that more horizontal continuity shallows the geometry and increases the the time required for a brine-to-freshwater interface to reach a new position following a change in recharge. These model results suggest that it is important to consider how differences in subsurface porosity impact the response time and the extent of saline intrusion for deserts as well as any other areas that might have salty groundwater.

1 Introduction

Numerical simulations of density-dependent flow assess the risk of saline groundwater intrusion in coastal areas (Meng et al., 2002; Trabelsi et al., 2013; J. W. Heiss & Michael, 2014), and in arid and often endorheic basins where evaporation outpaces recharge and concentrates solutes in groundwater (Stein et al., 2019). The discrepancy in fluid density encourages the development of an interface where the denser brine underlies the less dense fluid to create a freshwater lens, which is commonly known as a brine-to-freshwater interface (Duffy & Hassan, 1988; Philip & van Duijn, 1996; Fan et al., 1996; Wooding et al., 1997; Houston et al., 2011). For interfaces located in arid and endorheic basins, the processes that control the geometry and sensitivity of such interfaces remain unconstrained (Tejeda et al., 2003; Vásquez et al., 2013). The global decline of groundwater storage in aquifers in endorheic basins (Wang et al., 2018) increases the need to refine density-dependent dynamics when coupled with perturbations in recharge in such environments (Condon & Maxwell, 2019).

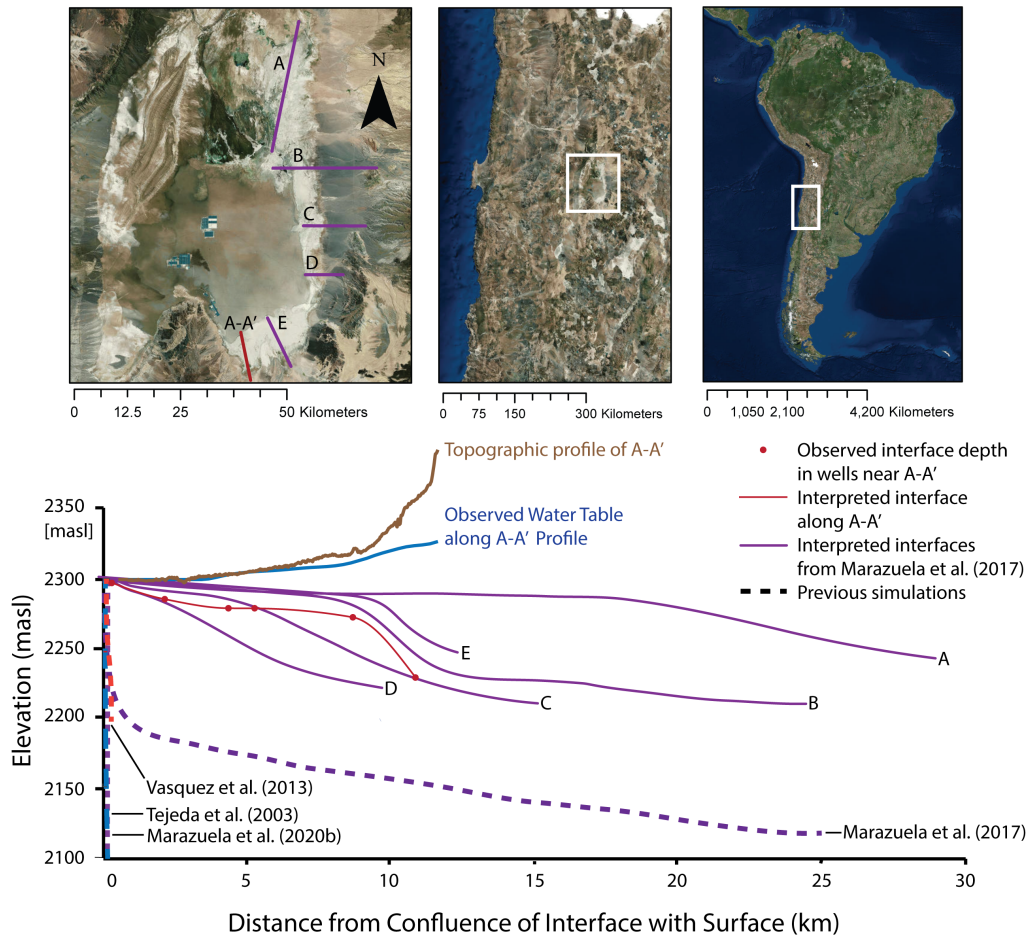


Figure 1. Comparison of observed 2-D interface locations with numerical simulations (dashed lines) of the interface along the transitions zone of SdA. Observed interfaces A-E (purple solid lines) from Marazuela et al. (2017) with locations along the eastern margin of the salar, as seen in the reference map in the upper left corner. The observed interface for this study along the A-A' transect is the solid red line.

65 The Ghyben-Herzberg approximation (Morgan et al., 2012) serves as a simple analytical
 66 solution to approximate the geometry of the brine-to-freshwater interface (Post et al., 2018),
 67 but it cannot account for time-dependent dynamics of density-dependent flow. Numerical simulations
 68 represent a tool for time-dependent analysis of saline intrusion, but simulations of saturated
 69 subsurface density-dependent fluid flow in homogeneous porous media do not ubiquitously
 70 capture the interface's geometry under realistic hydraulic conditions due to influences
 71 from heterogeneity (Post et al., 2007). Density-dependent numerical simulations of brine-to-
 72 freshwater interfaces in arid basins have either been homogeneous (Vásquez et al., 2013; Tejada
 73 et al., 2003) or simply layered models of local geology that underestimate basin-scale hetero-
 74 geneity and produce unrealistic results of the modeled interface (Marazuela et al., 2018). Pre-
 75 vious geostatistical modeling documented the influence of subsurface heterogeneity on sea-
 76 water circulation in coastal aquifers (Michael et al., 2016; Geng et al., 2020; Kreyns et al., 2020).
 77 However, the extent to which the continuity of subsurface heterogeneity impacts time-sensitive
 78 dynamics in general and the interface geometry for aquifers in arid basins specifically remains
 79 unconstrained.

80 This paper documents that heterogeneity influences both the steady-state geometry of the
81 brine-to-freshwater interface and the time-sensitive reaction of the interface in response to per-
82 turbations in recharge. Salar de Atacama provides an ideal site for assessing the role of het-
83 erogeneity because of its complex structural history (Reutter et al., 2006) and extensive de-
84 velopment of evaporite sequences (Jordan et al., 2004). The interface between brine and lat-
85 erally inflowing freshwater has a shallow geometry that has not been captured by previous mod-
86 eling of density-driven flow in the basin (Figure 1). A geostatistical approach with equally prob-
87 able distributions of hydraulic conductivity (K) based on field data from SdA provides a means
88 for investigating the role of continuity in heterogeneous geology on density-driven dynamics.
89 This represents the first attempt to constrain the impact of subsurface heterogeneity on brine-
90 to-freshwater interface geometry for arid and endorheic basins specifically. Our findings are
91 also the first definition of time-sensitive response of saline intrusion to perturbations in recharge
92 in relation to variations in continuity.

93 **2 Background**

94 **2.1 Hydrogeologic setting of salars**

95 Salars ("salt flats") comprise brine-bearing aquifers with subsurface heterogeneity in porous
96 media and distinct hydrologic dynamics. Salars primarily consist of evaporites in basins with
97 an annually negative hydrologic budget on average (Rosen, 1994; Tyler et al., 2006; Hernández-
98 López et al., 2014). Endorheic basins provide an ideal environment for evaporite accumula-
99 tion due to their tendency to inhibit the effective discharge of incoming sources (Eugster, 1980;
100 Houston et al., 2011), but salars also occur in open basins with a negative water budget (Rosen,
101 1994). Brine that is more saline than seawater (>35 ppt) can occur, and the higher discrep-
102 ancy in density results in a relatively shallower slope in the interface between the brine and
103 freshwater (Yecheili, 2000). Salars can develop a range of stratigraphically complex aquifers
104 because their climate-sensitive change in areal extent can create a series of interbedded litholo-
105 gies (Houston, 2009), as specifically documented in Munk et al. (in review). Since brine-bearing
106 aquifers commonly exist in tectonically active endorheic basins (Yager et al., 2017), faulting
107 among lithologies further complicate the lateral continuity of subsurface heterogeneity and pro-
108 duce interface geometries that defy theory when intersecting fault systems (Yecheili, 2000).
109 This study therefore provides a sensitivity analysis for investigating the role of heterogeneity
110 in density-dependent dynamics of such aquifers.

111 Aquifers in these environments also exhibit recharge-controlled water table configura-
112 tions (Haitjema & Mitchell-Bruker, 2005). The resulting lateral inflow dominates long-term
113 recharge as predicted by the Toth flow model (Rissman et al., 2015; Qureshi, 2011; Carmona
114 et al., 2000), which can include groundwater flow into a topographically separate and relatively
115 upgradient basin (Maxey, 1968; Schaller & Fan, 2009; Montgomery et al., 2003). Therefore,
116 while surface recharge provides a mechanism for sustaining groundwater levels (Boutt et al.,
117 2016) and solute delivery (Munk et al., 2018), lateral subsurface inflow represents the long-
118 term recharge mechanism (Scanlon et al., 2006; Houston, 2009; Ye et al., 2016). Basin-scale
119 recharge trends in arid climates can change over relatively short (i.e. interdecadal and millen-
120 nial) timescales (Placzek et al., 2009), highlighting the importance of considering climate-driven
121 shifts even if short-term hydrology appears to be stable (Zhu et al., 1998). To date, there has
122 been no study that has characterized the impact of heterogeneity on the time-sensitive response
123 of brine-to-freshwater interfaces to perturbations in subsurface lateral inflow (Sanford & Pope,
124 2010; Ferguson & Gleeson, 2012). The framework for the numerical simulations include sub-
125 surface lateral inflow as the main source of recharge and evaporation at the margin of the mod-
126 eled salar as the primary source of discharge.

127 **2.2 Sensitivity analyses on density-driven flow systems**

128 Many studies have documented and simulated density-dependent flow and its resulting
129 brine-to-freshwater interface in both coastal (Yecheili, 2000; Werner & Simmons, 2009; Tra-

130 belsi et al., 2013) and inland aquifers (Fan et al., 1996; Wooding et al., 1997; Tejada et al.,
131 2003). Studies that numerically assess the factors that impact saline intrusion commonly ex-
132 amine a single influence on the interface's dynamics, such as changes in recharge (Post et al.,
133 2019) or discharge (Werner & Simmons, 2009). For coastal aquifers, studies primarily focus
134 on coupling density-dependent flow with solute transport in order to define the risk of saline
135 groundwater intrusion to inland groundwater resources (Meng et al., 2002; Werner & Simmons,
136 2009; Morgan et al., 2012). Such studies frequently investigate the sensitivity of brine-to-freshwater
137 interface migration via solute transport coupled with various influences, including but not lim-
138 ited to the buoyancy effect from density-depedent flow (Bear, 1972; Werner et al., 2013), wave-
139 induced groundwater circulation cells (J. Heiss et al., 2017), fluctuating circulation from tidal
140 forcing (J. W. Heiss & Michael, 2014; Bailey, 2015), variations in circulation cell size from
141 bedform topography (Konikow et al., 2013), increased landward interface migration from sea
142 level rise (Yechieli et al., 2010; Ketabchi et al., 2016), increased supratidal salinity from evap-
143 oration (Geng & Boufadel, 2015), increased interface migraton via preferential pathways from
144 conducive faulting (Trabelsi et al., 2013), anthropogenic pumping of inland fresh groundwa-
145 ter (Ferguson & Gleeson, 2012), and heterogeneity in geologic media (Michael et al., 2016;
146 Michael & Khan, 2016; Liu et al., 2014; Mahmoodzadeh & Karamouz, 2019). While stud-
147 ies of saline groundwater intrusion primarily focus on coastal environments, inland and arid
148 basins are also prevalent sites of brine development (Rissman et al., 2015) and comprise evaporite-
149 dominated geology and arid geomorphology that is unique from coastal environments and yet
150 remains uncomprehensively modeled on a global scale (Houston et al., 2011). Specifically for
151 inland and arid basins, studies of density-dependent flow primarily utilize analytical methods
152 or numerical simulations to document groundwater circulation within steady state conditions
153 without considering either variations in steady-state conditions or transient responses to per-
154 turbations in recharge (Duffy & Hassan, 1988; Fan et al., 1996; Wooding et al., 1997; Hamann
155 et al., 2015).

156 **2.3 Numerical simulations of density driven flow & heterogeneity**

157 Since geologically heterogeneous media comprise the majority of aquifers (Gelhar et al.,
158 1992), many numerical studies have investigated the impact of subsurface heterogeneity on density-
159 dependent flow dynamics in order to elucidate more realistic mechanistic explanations for the
160 documented salinity distributions and transport flowpaths (Schincariol et al., 1997), especially
161 for coastal aquifers (Russoniello et al., 2013). Among them, Sawyer et al. (2014) establish that
162 hydraulically conducive stratigraphic features can control geochemical fluxes in near-shore aquifers.
163 Michael et al. (2016) provide an extensive analysis on the impact of geologic heterogeneity
164 on seawater circulation, while Kreyns et al. (2020) document that freshwater discharge can ex-
165 tend further offshore in heterogeneous volcanic aquifers when compared to homogeneous coun-
166 terparts. (Geng et al., 2020) use simulations to investigate the impact of subsurface hetero-
167 geneity on tidally-influenced circulation, thereby confirming the importance of coupling het-
168 erogeneity with influences on an aquifer's hydrologic dynamics in order to further constrain
169 geologic impacts on solute transport. Michael and Khan (2016) further detail heterogeneity's
170 influence on variable solute transport and decreased travel time through an aquifer in response
171 to relatively deeper groundwater pumping. While freshwater aquifer storage in coastal aquifers
172 may experience a multi-decadal time lag response due to changes in recharge resulting from
173 fluctuations in brine-to-freshwater interface migration (Klammler et al., 2020), the impact of
174 continuity in heterogeneity on further increasing such a time lag but remains unconstrained.
175 This study therefore aims to further define how continuity in basin-scale heterogeneity impacts
176 the time sensitivity of density-dependent response to perturbations in recharge.

177 Given the resource-rich importance (Kunasz, 1980; Munk et al., 2016) and prevalence
178 of brine-bearing aquifers underlying inland and arid basins (Yechieli & Wood, 2002; Wang et
179 al., 2018), simulating density-dependent flow in these systems has increased in recent years.
180 These basins' unique hydrologic conditions, such as lack of tidal influence and distinct evap-
181 oration patterns (Hernández-López et al., 2014), further elevate the need for environment-specific
182 modeling. Simulations of density-dependent dynamics in arid, inland basins commonly model

183 either homogeneous conditions (Tejeda et al., 2003) or simple stratigraphic interpretations with
184 continuous, single-layer aquitards (Duffy & Hassan, 1988; Marazuela et al., 2018). While Marazuela
185 et al. (2018) document the shallowing of the interface which presumably results from an un-
186 derlying lower-K confining unit, the resulting modeled interface does not capture realistic ge-
187 ometry (Figure 1). While continuity in stratigraphic units' hydraulic conductivity increases saline
188 groundwater circulation (Michael & Khan, 2016), the degree to which basin-scale hydrostrati-
189 graphic complexity influences salinity distributions and thus brine-to-freshwater interface ge-
190 ometry remains unclear for arid basins (Houston et al., 2011). The series of numerical sim-
191 ulations presented here represent the first attempt to characterize the impact of heterogeneity
192 on brine-to-freshwater interface geometry for arid and inland basins specifically, as well as pro-
193 vide insight on the impact of heterogeneity on density-dependent dynamics to changes in recharge
194 for brine-bearing aquifers in general. This work is highly important because of the need to un-
195 derstand the interplay of freshwater and underlying saline water as these basins have contin-
196 ued pressures put on freshwater and resource extraction.

197 3 Simulations

198 Saturated density-dependent groundwater flow was simulated using SEAWAT, a cell-centered
199 finite difference approximation that solves both saturated fluid flow and solute transport (Langevin
200 & Guo, 2006). To address the role of heterogeneity on brine-to-freshwater interface sensitiv-
201 ity, we use a geostatistical approach with a series of realizations of K fields by kriging avail-
202 able hydrogeologic data for SdA with a Markov approach using T-PROGS software (Carle, 1999).
203 We base the transition probabilities for the K distributions on the lithologies documented from
204 diamond drill cores recovered from the southeastern margin of SdA (S1). To address the site-
205 specific implications for SdA, a separate hydrostratigraphic framework (HSF) was developed
206 for the A-A' transect noted in Figure 1 where brine underlying the salar interacts with shal-
207 low subsurface laterally inflowing freshwater to create a brine-to-freshwater interface along
208 the southeastern margin (Figure S2). The HSF relies on a geologic model that was developed
209 from core and well data, geophysical surveys, and knowledge of surface geology and basin struc-
210 ture based on previous literature (Jordan et al., 2002; Lowenstein et al., 2003; Mpodozis et al.,
211 2005; Reutter et al., 2006), as further described in the supplementary section (S1) as well as
212 filed observations by the authors.

213 3.1 Boundary & initial conditions

214 The finite grid and boundary conditions for the simulations are based on representations
215 of aquifer characteristics for the modeled basin, including recharge via subsurface lateral in-
216 flow, discharge via ET, and topography based on the A-A' transect (Figure 1). Excepting changes
217 in recharge and the K distributions, all other physical boundary and initial conditions remain
218 constant. Figure 3 illustrates initial and boundary conditions. The domain is 13,000 m long
219 by 300 m deep, and is discretized into 100 m long by 10 m deep grid cells. The framework
220 represents one side of a basin because the hypothetical symmetry of a basin renders the sim-
221 ulation of both sides redundant and therefore unnecessary. The surface boundary is based on
222 smoothed elevation models of the topography at SdA from the available 10 meter-resolution
223 digital elevation data. A Dirichlet boundary represents specified head for the modeled edge
224 of the nucleus, which is approximately 1 m below the modeled nucleus surface. The entire left
225 side of the model domain that represents the edge of the nucleus has a constant dissolved salt
226 concentration of $0.2 \text{ g}\cdot\text{cm}^{-3}$ which represents the maximum concentration observed in highly
227 saline brines. A Neumann boundary condition represents the modeled subsurface laterally in-
228 flowing flux of freshwater on the right side of the model domain has no concentration of dis-
229 solved salt. Discharge is represented as evaporation via a head-dependent flux that equates
230 to an equivalent flux of the baseline inflow flux of $500 \text{ m}^3\cdot\text{d}^{-1}$ if the hydraulic head is less than
231 1 meter from the modeled surface (Figure 3). All other boundaries not otherwise described
232 have no flux in either fluid or solute. The initial solute concentration for the entire extent of
233 the domain is $0 \text{ g}\cdot\text{cm}^{-3}$. Initial hydraulic head is a uniform 1 m below the modeled surface.

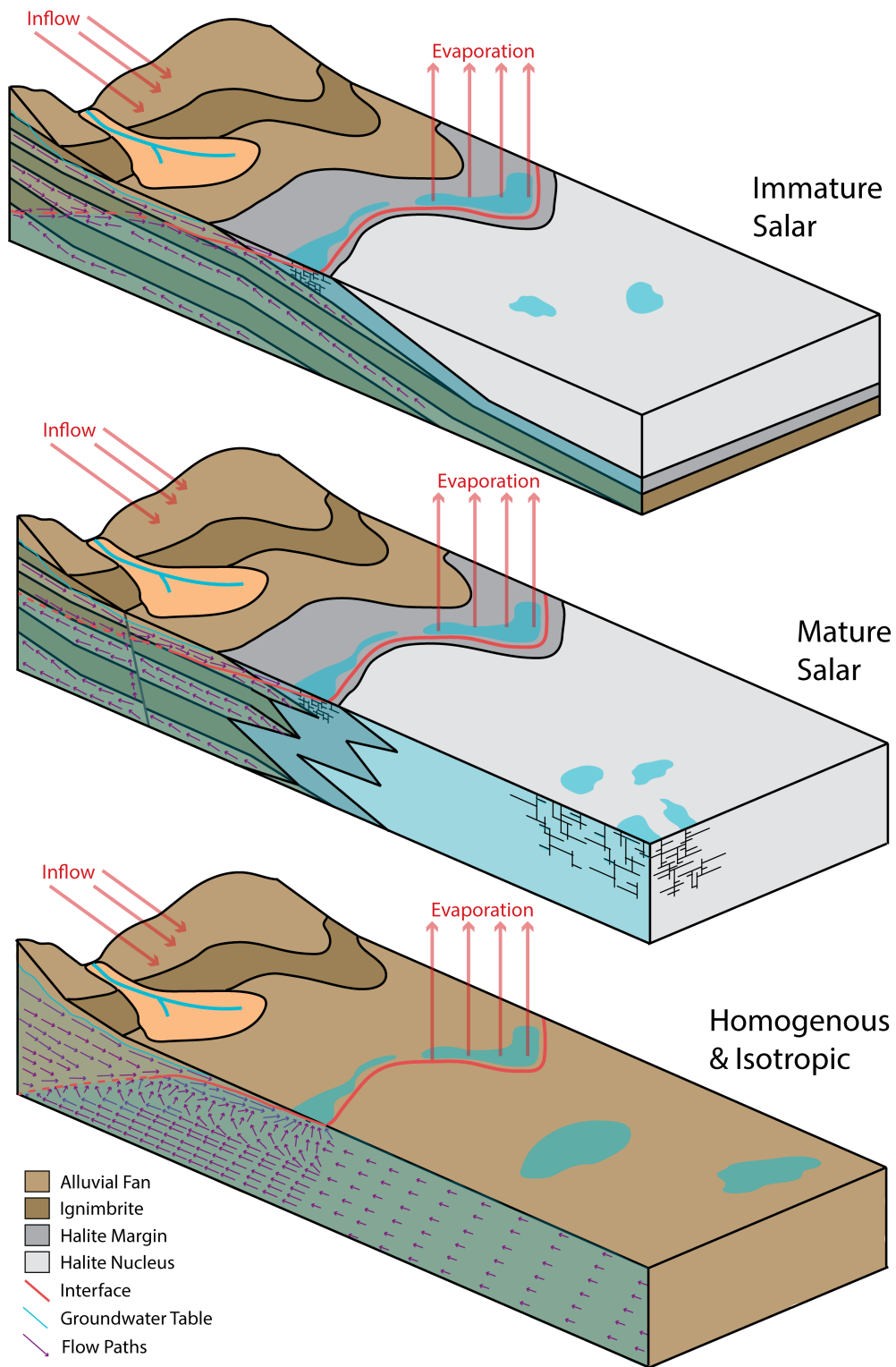


Figure 2. Conceptual illustration of mature versus immature salars and their homogeneous counterpart, with the resulting brine-to-freshwater interface and flow vectors. Adapted from Houston et al. (2011).

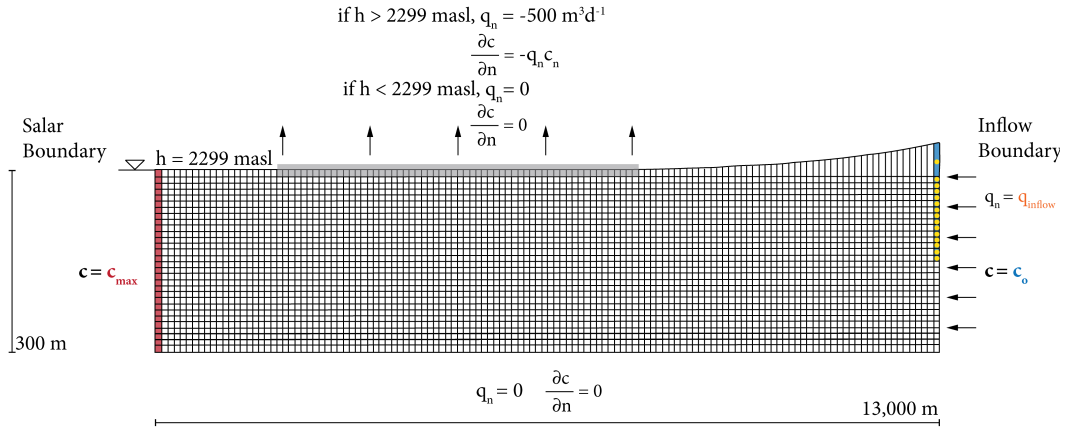


Figure 3. Boundary conditions for the 300 m deep by 13,000 m long 2-D model framework with a vertical exaggeration of 10. Note that the model is discretized into 30 by 130 cells each cell having the dimensions of 10 m deep by 100 m wide. Also note that $c_{\max} = 0.2 \text{ g}\cdot\text{cm}^{-3}$, $c_o = 0 \text{ g}\cdot\text{cm}^{-3}$, and that q_{inflow} varies by 300, 500, and $700 \text{ m}^3\cdot\text{d}^{-1}$. Vertical exaggeration is 10.

Parameter	Value	Unit
Domain length	13,000	m
Domain thickness (B)	300	m
Longitudinal dispersivity (α_L)	10	m
Horizontal transverse dispersivity (α_H)	1	m
Vertical transverse dispersivity (α_V)	0.01	m
Diffusion coefficient	$1\cdot 10^{-6}$	$\text{m}^2\cdot \text{s}^{-1}$
Effective porosity (ϑ)	0.3	-
Constant head at nucleus boundary	2299	masl
Freshwater density (ρ_o)	1	$\text{g}\cdot\text{cm}^{-3}$
Brine density (ρ_{\max})	1.2	$\text{g}\cdot\text{cm}^{-3}$
Storativity (S_s)	$1\cdot 10^{-4}$	m^{-1}
Specific yield (S_y)	0.02	-
Vertical anisotropy (K_h/K_v)	10	-

Table 1. Constant boundary conditions for the numerical modeling approach. These conditions are constant throughout the modeled time for every model. Note that the listed vertical anisotropy value applies for the non-isotropic models.

234 Values of longitudinal, horizontal transverse, and vertical transverse dispersivity in all mod-
 235 els are 10 m, 1 m, and 0.01 m respectively. These values are consistent with modeling aquifers
 236 of this scale (Gelhar et al., 1992). All iterations run with the above-described initial condi-
 237 tions to $3\cdot 10^6$ days. The models then run for another $3\cdot 10^6$ days following a perturbation in
 238 hydrologic conditions in order to assess the sensitivity of the brine-to-freshwater interface. Ta-
 239 ble 1 lists the constant boundary conditions for the numerical simulation.

240 3.2 Simulating perturbations in recharge

241 Groundwater inflow is the only boundary condition in this study that experiences vari-
 242 ation for every realization of K. The simulations were run to an initial steady state with no in-
 243 terface movement in order to establish an interface geometry from initial conditions. Each re-

alization is subsequently exposed to three different recharge scenarios as step functions: an increase in recharge ($700 \text{ m}^3 \cdot \text{d}^{-1}$), an equal decrease in recharge ($300 \text{ m}^3 \cdot \text{d}^{-1}$), and no perturbation in recharge ($500 \text{ m}^3 \cdot \text{d}^{-1}$). The development of the boundary condition representing recharge is based on the assumption that arid hydrology relies on interbasin flow that is characterized by long residence times and therefore prolonged variations in recharge, as supported by site-specific data (Houston, 2009; Ortiz et al., 2014; Corenthal et al., 2016). While previous numerical studies have included direct recharge (Marazuela et al., 2018), the impact of direct recharge is not considered in this study because arid basins exhibit minimal to no surficial recharge where ET outpaces precipitation rates (Scanlon et al., 2006) and the dominant recharge mechanism of such basins is lateral groundwater flow following the Toth model (Schaller & Fan, 2009).

3.3 Distributions of hydraulic conductivity

Geostatistic realizations of heterogeneous distributions were based on K values assigned to lithostratigraphic units from the study site in the southeastern margin of SdA. The hydraulic conductivity values are based on correlating geologic and hydraulic data from the 29 cores (Table S1) and 48 wells (Table S2) from within the approximately 130 km^2 area that comprises the southeastern margin of SdA. The hydrostratigraphic correlation is based on over 50 hydraulic tests that have occurred in the area. Hydrostratigraphic interpretations were separated into five lithologic facies based on the conceptualization in Munk et al. (in review): medium-grain clastic from alluvial fan deposits ($10 \text{ m} \cdot \text{d}^{-1}$), fine-grain carbonate ($1 \text{ m} \cdot \text{d}^{-1}$), vuggy carbonate ($100 \text{ m} \cdot \text{d}^{-1}$), un-fractured ignimbrite ($0.01 \text{ m} \cdot \text{d}^{-1}$), and interbedded gypsum and carbonate ($0.1 \text{ m} \cdot \text{d}^{-1}$). K values were determined within one standard deviation from the average K value for each lithostratigraphic facies. For all realizations, the proportions for fine carbonate, alluvial fan deposits, ignimbrite, vuggy carbonate, and gypsum were 43, 24, 19, 8, and 6 percent, respectively.

Three groups of realizations with distinct horizontal to vertical stratigraphic continuity ratios (c_h/c_v) were created to address the role of geologic complexity in the geometry and time sensitivity of interface response: equal continuity in both directions ($c_h/c_v=1$), increased horizontal continuity by a factor of two ($c_h/c_v=2$), and increased horizontal continuity by a factor of three ($c_h/c_v=3$). 38 realizations of K were created for each group. The K_{eff} values for the realizations range within $5.3 \text{ m} \cdot \text{d}^{-1}$ and $20.3 \text{ m} \cdot \text{d}^{-1}$, according to Darcy flux estimates.

3.4 Metrics for assessing interface geometry, sensitivity & stability

For each simulation, velocity vectors, solute concentration, and hydraulic head values were collected for every time step. From these results, four metrics were used to assess differences in interface geometry and the time-sensitive response in the simulation results. The first metric is the average slope of the interface, which was assessed with a linear best fit for each simulated interface after reaching an initial steady state. The second metric is the horizontal width of transition zone between fresh (i.e. $<0.04 \text{ g} \cdot \text{cm}^{-3}$) and highly saline (i.e. $>0.18 \text{ g} \cdot \text{cm}^{-3}$) groundwater [L]. Third, the length of the interface's migration in the horizontal direction [L] provides a metric for assessing the sensitivity of the interface following a change in recharge to the modeled aquifer. Fourth, the time-sensitivity of the interface's response following a perturbation in recharge is characterized by a time constant as defined by:

$$\frac{[m]_f}{[m]_i} = e^{-kt} \quad (1)$$

where the rate of change in the mass of solute is equal to an exponential curve (i.e. "e-folding time"). This response is assessed via the rate of change in the total mass of modeled solute in the domain. For the purpose of this study, the e-folding time serves as a characteristic of the response rate, with the amount of time corresponding to the relative speed of response to a perturbation in recharge. We additionally assess flow topology using the Okubo-

Weiss (OW) method to provide a mechanistic explanation for the simulation results (de Barros et al., 2012; Geng et al., 2020).

4 Results

4.1 Geometry & dynamic response of the hydrostratigraphic framework of Salar de Atacama

Figure 4 illustrates the solute concentration values, hydraulic head field, and velocity field of both the HSF of SdA and the homogeneous model that represents the K_{eff} of the HSF. For the homogeneous results, solute concentration values show a consistent transition zone width from 0 to $0.2 \text{ g}\cdot\text{cm}^{-3}$ with depth, though the upper 50 meters of the model near the area of modeled evaporation appears to increase in transition zone width. The hydraulic head and flow velocity fields reflect the geometry of concentration values, with higher head and velocity values at depth in the modeled inflowing freshwater, forcing fluid convection and upwelling. Both the hydraulic head and velocity fields have a spatially even distribution in the gradual decline from highest to lowest values at depth. Concentration values in the homogeneous model diverge from observed field conditions by several kilometers at depth.

Compared to its homogeneous counterpart, results from the heterogeneous model that represent the HSF of SdA have a shallower interface that conforms with observed concentration values within 10 meters at depth. Numerical results shown in Figure 4 also indicate a varying width of the brine-to-freshwater transition zone from sharp to diffuse. The hydraulic head field similarly expresses sharp to diffuse transitions from high to lower values. Despite the variations in hydraulic head at depth, the majority of the high flow velocity is concentrated in the upper surficial layer of the domain and coincides with the laterally inflowing recharge. The e-folding time in response to inflow perturbations is larger by at least a factor of three for the HSF model when compared to the homogeneous model (Figure 8). The total distance that the interface travels as a result of a change in inflow, as assessed through the movement of the 0.5 isoconcentration line, likewise exhibits a distinct difference between the heterogeneous and homogeneous models, with interface travel through permeable pathways within the heterogeneous model.

4.2 Geometry & dynamic response of the geostatistical realizations of hydraulic conductivity to changes in inflow

Simulations with equally probable K distributions produce physical and time-sensitive results that diverge from their homogeneous counterparts and show a statistically significant relationship with stratigraphic continuity in a geologically complex environment (Table 2). The simulations show interface geometries that decrease in slope as c_h/c_v increases (Figure 6). The range of locations for the interface for each group of geostatistic realizations is shown in Figure 7. Homogeneous models with equivalent K_{eff} as the realizations produce interface geometries that are steeper by at least a factor of two and in some cases by an order of magnitude. The average slope for each group of realizations increases by approximately half a degree for every increase in c_h/c_v by a factor of one. Similarly, the thickness of the transition zone between saline and freshwater also has a pattern of generally decreasing while expressing more variation in diffuse versus sharp concentration gradients as horizontal continuity increases, whereas the homogeneous models show a consistently thicker transition zone (Figure 8).

The density-dependent dynamics in the geostatistical realizations exhibit a pattern for the sensitivity of the interfaces. Increased c_h/c_v in the realizations yields an increase in the overall length of interface migration and thus presumably creates an increase in the response of density-dependent flow to changes in subsurface later inflow into an aquifer. An increase in the horizontal continuity also results in longer time constants in the exponential decay of an interface's migration rate (Figure 9). From least to most continuous, each group of realizations respectively yielded average interface migration of $3586 \pm 2323 \text{ km}$, $3816 \pm 1679 \text{ km}$, and

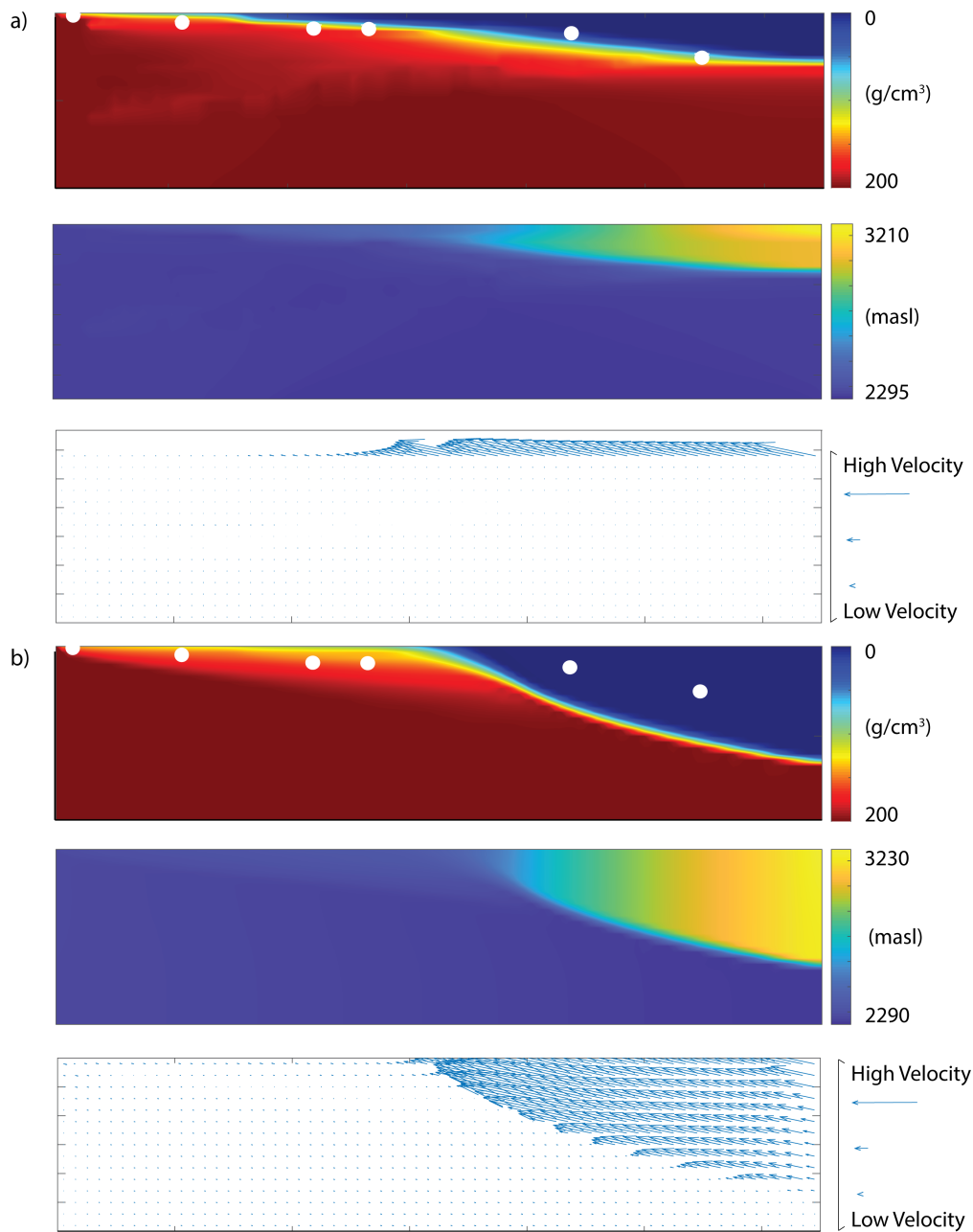


Figure 4. Visual comparison of the distribution of concentration ($\text{g}\cdot\text{cm}^{-3}$) of dissolved salt in the modeled aquifer, the hydraulic head, and the velocity vectors for both the a) heterogeneous model based on the hydrostratigraphic framework and b) the homogenous model with the same K_{eff} . White dots indicate the location of the observed interface in the wells.

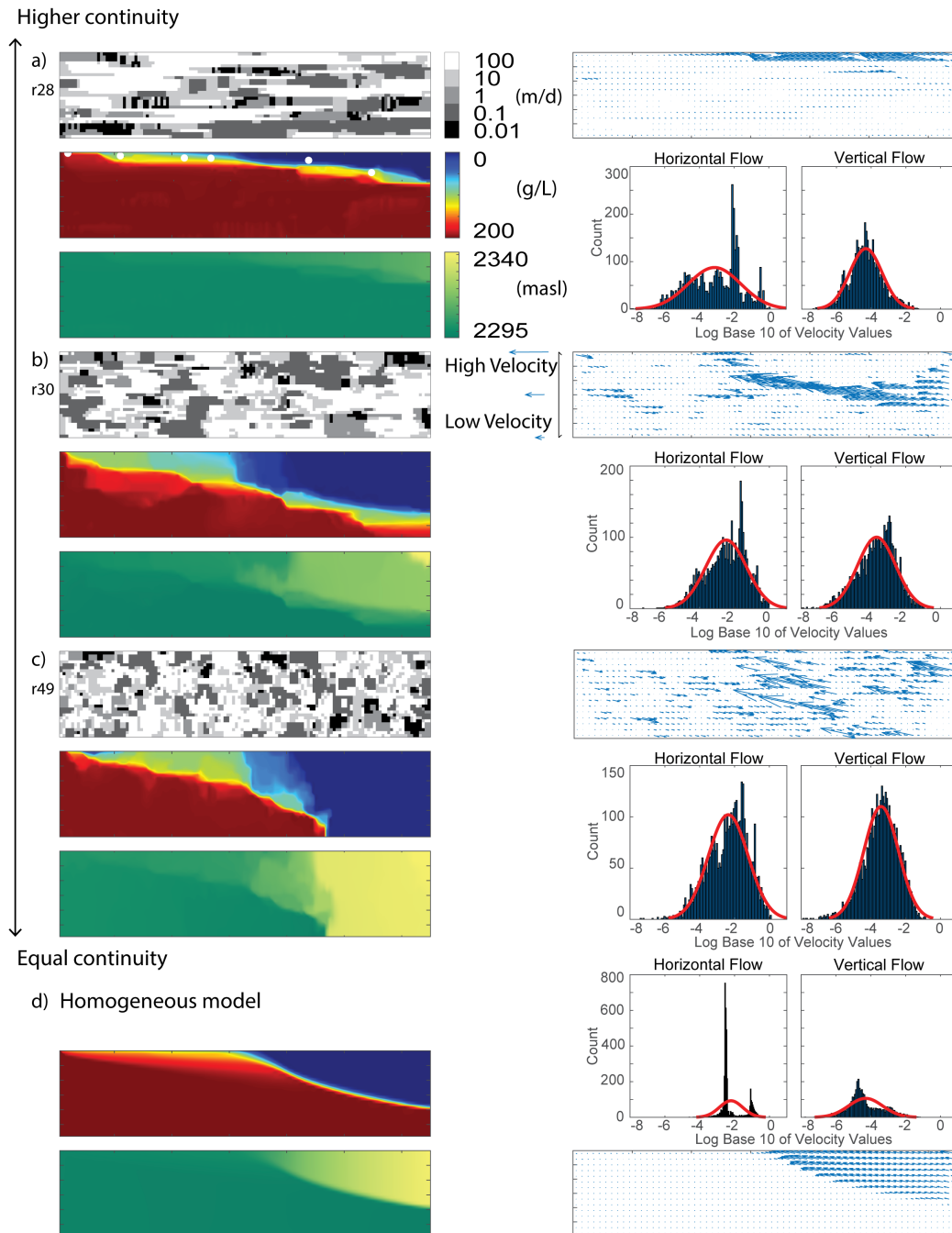


Figure 5. Results for one example in each group of K realizations, with a) $c_h/c_v=3$, b) $c_h/c_v=2$, c) $c_h/c_v=1$, and d) homogeneous model. For each example, clockwise from the upper left corner, the K distribution in m/d, flow velocity vectors, flow velocity distribution (\log_{10} m/d), hydraulic head distribution (masl), and salinity distributions (g/L) are shown. White points are observed interface locations.

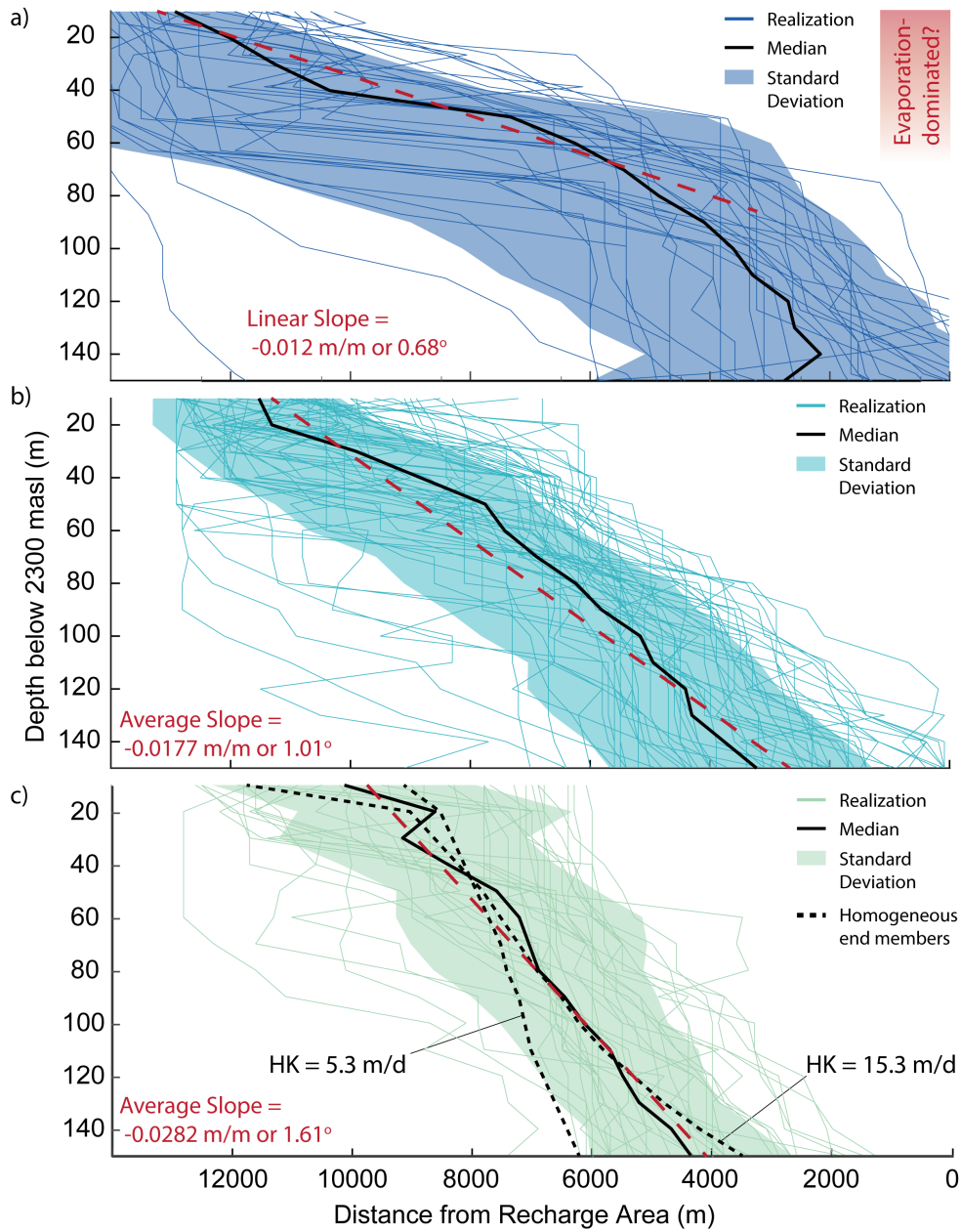


Figure 6. Distance of the 0.5 concentration point from the recharge area with depth for each group of geostatistical of hydraulic conductivity. Each group of realizations is separated based on degree of continuity, with increased horizontal continuity by a factor of three (dark blue), increased horizontal continuity by two (light blue), and equal continuity (green) in order from top to bottom. The value for the linear best fit (dashed red) for the median (solid black) of each group is listed in the lower right corner of the graphs. The shaded region is the standard deviation.

Metric	Increase v. Decrease	Group Comparison	Result	Critical Value	Significance Level
Geometry	-	1 and 2	4.53	1.67	0.05
Geometry	-	2 and 3	3.70	1.66	0.05
Geometry	-	1 and 3	6.15	1.67	0.05
Time Constant	Increase	1 and 2	0.38	1.3	0.1
Time Constant	Increase	2 and 3	1.48	1.3	0.1
Time Constant	Increase	1 and 3	1.75	1.66	0.05
Time Constant	Decrease	1 and 2	1.05	1.3	0.1
Time Constant	Decrease	2 and 3	1.46	1.3	0.1
Time Constant	Decrease	1 and 3	2.72	1.66	0.05

Table 2. Statistical significance of variance in metrics by group of HK realizations, with the result and corresponding critical value and significance level. Metric results related to recharge increase versus decrease noted where applicable. Groups are distinguished by c_h/c_v value.

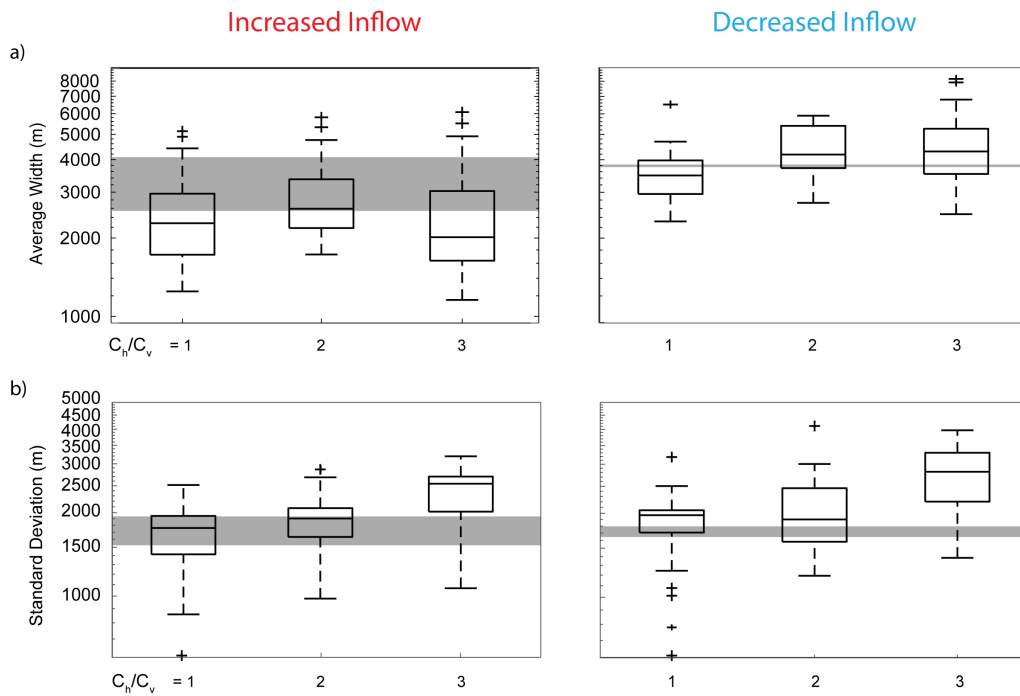


Figure 7. The distribution of a) the average and b) the standard deviation of transition zone widths from brackish ($0.04 \text{ g}\cdot\text{cm}^{-3}$) to brine ($0.18 \text{ g}\cdot\text{cm}^{-3}$) for the geostatistical realizations of hydraulic conductivity, separated based on horizontal hydrostratigraphic continuity as compared to vertical continuity. Gray shaded area is the range of homogeneous values.

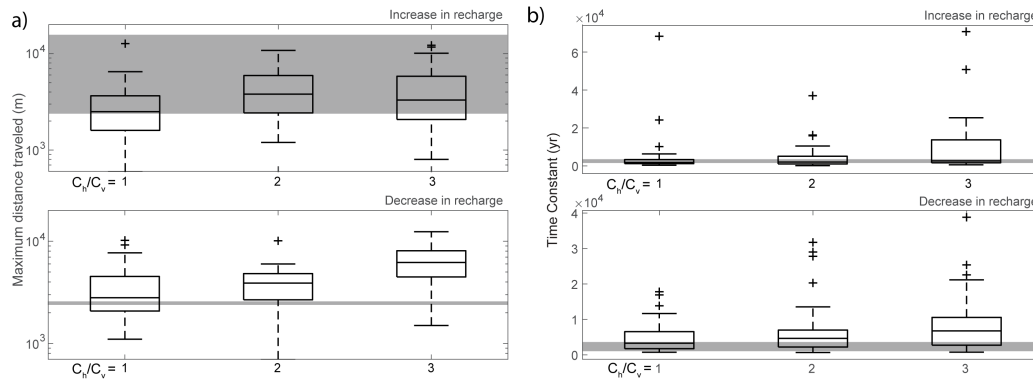


Figure 8. The distribution of a) maximum distance of interface travel and b) time response to a change in inflow for the geostatistical realizations of hydraulic conductivity, separated based on C_h/C_v . Above statistical analysis represent an increase in inflow and the lower plots represent results from a decrease in inflow. The gray shaded area indicates the homogeneous model results.

339 6548 ± 2926 km following a decrease in recharge. This equals an increase of 48% and 31%
 340 in average migration for each respective increase in c_h/c_v . For e-folding times in the interface
 341 response, the average time constant was 4804 yr, 5754 yr, and 9881 yr for each group from
 342 least to most in c_h/c_v , creating a 20% and 72% increase in time for each respective increase
 343 in c_h/c_v . The observed time response differences are statistically significant between the groups
 344 $c_h/c_v=1$ and $c_h/c_v=3$ to a significance level of 0.1; between groups $c_h/c_v=1$ versus $c_h/c_v=3$ and
 345 $c_h/c_v=2$ and $c_h/c_v=3$ to a significance level of 0.05 (table 2). Comparatively, the brine-to-freshwater
 346 interface migration within the homogeneous models exhibit less sensitivity in terms of the amount
 347 of interface movement and decreased time required to reach a new steady state subsequent to
 348 being exposed to the same perturbations in recharge.

349 5 Discussion

350 5.1 Geometry & inferred density-driven dynamics of the brine-to-freshwater inter- 351 face at Salar de Atacama

352 This study represents the most robust attempt to numerically simulate and accurately cap-
 353 ture the geometry of the brine-to-freshwater interface along the southeastern margin of the halite
 354 nucleus at SdA. It also represents the most accurate 2-D hydrostratigraphic interpretation of
 355 the southeastern margin. Simulation results of the K field resulting from the hydrostratigraphic
 356 interpretation suggest that subsurface heterogeneity impacts density-dependent dynamics to the
 357 degree that it shallows the interface geometry and focuses flow where the interface intersects
 358 conduits of relatively higher K. Focused discharge represented by the modeled velocity val-
 359 ues occur along highly continuous preferential pathways, further suggesting that continuity in
 360 hydrostratigraphic units may serve as a controlling factor in the impact of heterogeneity. These
 361 results therefore provide a basis for investigating not only the role of heterogeneity, but specifi-
 362 cally the degree to which conductivity impacts density-dependent dynamics and associated
 363 solute transport. While the motivations behind previous simulations of the basin may not have
 364 included the creation of an accurate density-dependent basin-scale simulation, results from this
 365 study suggest that locating and defining the locations and prevalence of hydraulically conducive
 366 media hold value in defining density-dependent dynamics (Marazuela et al., 2018). Thus site-
 367 specific observations potentially represent a relationship between heterogeneity and density-
 368 dependent sensitivity to perturbations in recharge that require further investigation, which is
 369 what this current work presents.

5.2 Impact of increased hydrostratigraphic continuity in heterogeneity on density-driven dynamics & resulting interface sensitivity

Results from the series of K realizations demonstrate that horizontal continuity in hydrostratigraphic heterogeneity decreases the slope of the brine-to-freshwater interface (Figure 6). The decreased interface slope results from decreased vorticity-dominated flow, as indicated by OW values (Figure 9). The simulations also support that increased horizontal continuity in hydrostratigraphic units generally decrease the average thickness of the transition zone, while also increasing the variability between a sharp and diffuse transition zone (Figure 7). This supports previous findings of variably diffuse behavior of brine-to-freshwater interfaces in heterogeneous media (Michael et al., 2016). Increased variability in transition zone thickness likely results from increased preferential pathways in the horizontal direction, which is supported by the increased prevalence of strain-dominated flow in areas where the interface intersects conduits of flow (Figure 9). Since increased versus decreased perturbations in recharge have distinct effects on the thickness of the transition zone, it is important to account for different mechanisms involved in the physical expression of an interface. Increased recharge does not impact the average transition zone thickness because the majority of interface movement is controlled by the interplay between head and density gradients, while decreased recharge results in all model results exhibiting similar average transition zone thickness regardless of horizontal hydrostratigraphic continuity because diffusion is a primary mechanism for solute transport.

The simulated interface responses to changes in hydraulic head are consistent with previous density-dependent interface modeling where the interface adjusted in location based on hydraulic head variations (Yecheili, 2000; Yecheili et al., 2001; Liu et al., 2014). This study further indicates that increased hydrostratigraphic continuity increases density-driven sensitivity of groundwater flow in terms of the extent of interface travel and the time-sensitive response for the interface to reach a new dynamic steady state following a perturbation in recharge (Figure 8). The shift of the simulated aquifer's density-driven dynamics toward more strain-dominated flow accounts for this change in sensitivity (Figure 9). The importance of continuity in heterogeneity is supported by comparison with homogeneous models, which have results that are comparatively limited in both length of interface movement and in the time-sensitive response, though they share the same K_{eff} and anisotropy values as the series of K realizations (Figure 8). The series of K distributions with $c_h/c_v=1$ result in similar time responses when compared to the homogeneous results because the connectivity of vorticity-dominated flow regimes at depth allow density-dependent flow to equilibrate at similar rates. Increasing horizontal continuity in hydrostratigraphy limits the vertical connectivity of vorticity-dominated flow regimes and promotes strain-dominated flow, which result in the prolonged density-driven response.

Horizontal continuity in hydrostratigraphic units controls flow topology in density-dependent dynamics, and this relationship is responsible for the resulting variable sensitivity of the interface. An increase in c_h/c_v leads to an increase in the prevalence of highly conductive preferential pathways in the horizontal direction which thus increases the potential for the disequilibrium of hydraulic head in vertical direction. Higher disequilibrium results in longer timescales required for density-dependent flow to reach a new stable position. Sensitivity likewise increases in terms of the length of interface migration because of increased preferential pathways facilitate sensitivity to density-driven hydraulic head variations and thus trigger strain-dominated flow where the interface meets high- K units. OW analysis suggests that strain-dominated flow is focused along the brine-to-freshwater interface where it intersects with high- K preferential pathways (Figure 9). The distribution of OW values also indicate elongated diffusion-dominated flow in the horizontal direction as c_h/c_v increases. These two observations indicate that while increased c_h/c_v creates horizontally elongated diffusive flow conditions that increase hydraulic disparities in the vertical direction and therefore decrease the response time for the system as a whole, the interface-specific locations of conduits for preferential flow host the density-dependent discrepancy in hydraulic head that drives the saline intrusion.

422 Simulated evaporation remained constant throughout the study, and an analysis of the
 423 impact of evaporation on the brine-to-freshwater interface sensitivity is beyond the scope of
 424 this study. However, it is possible to infer the potential impact from evaporation on the interface-
 425 based sensitivity analysis. A remarkably consistent characteristic of the response to changes
 426 in inflow was the relatively unchanged interface position within the modeled area of evapo-
 427 ration. When confluence with the surface intersected the evaporation area, interface migration
 428 in response to perturbations in recharge was smaller by almost an order of magnitude com-
 429 pared to the average length of migration of the cells at depth. This observation confirms the
 430 importance of considering potential evaporation in arid aquifers with abundant brine.

431 **5.3 Implications for future simulations & accurate physical expressions of brine-to-** 432 **freshwater interfaces in arid basins**

433 Increased horizontal hydrostratigraphic continuity creates brine-to-freshwater interface
 434 dynamics that shallow the interface and increase the variability in transition zone thickness,
 435 which differs from predictions based on homogeneous numerical simulations of density-dependent
 436 groundwater flow (Figure 10). The direct relationship between lateral hydrostratigraphic con-
 437 tinuity in subsurface heterogeneity and interface geometry indicates that heterogeneity repre-
 438 sents a primary control on brine-bearing systems with subsurface lateral recharge as the pri-
 439 mary long-term recharge mechanism. The relationship between horizontal continuity in ge-
 440 ologic heterogeneity and variability in transition zone thickness indicates that representations
 441 of hydrostratigraphic heterogeneity is valuable for realistic expressions of the interface thick-
 442 ness. This is especially critical for arid basins, where the development of transitional evap-
 443 orite facies creates locally continuous units (Vásquez et al., 2013). In salt flat environments,
 444 the prevalence of continuous boundaries of evaporite series against higher-permeability facies
 445 may account for the shallowing behavior of observed interfaces in certain locations where high
 446 evaporation dominates. Brine-bearing aquifers with continuous stratigraphic contacts between
 447 high and low permeability units may develop distinctly shallower interface geometries than tra-
 448 ditional homogeneous or simplistic models, where higher-K units act as high-K conduits for
 449 fluid flow. This is especially true for depositional environments and marginal zones adjacent
 450 to developed salars. These observations are particularly relevant to brine-bearing aquifers that
 451 do not experience additional hydraulic fluctuations like tidal forcing and wave-induced circula-
 452 tion, such as coastal aquifers.

453 This study also indicates evaporation as a control in interface expression in arid and in-
 454 land basins that highlight the necessity for high resolution of hydrostratigraphic accuracy in
 455 numerical simulations. Results indicate that the trend of an increasingly shallowing interface
 456 with increasing horizontal continuity is also prevalent in arid basins with high rates of evap-
 457 oration, where discharge controls the hydraulic head distribution and promotes vertical and up-
 458 wards fluid migration over any lateral sensitivity to recharge. This evaporation-dominant flow
 459 pattern occurs through the upper 50 meters in all simulations in this study. However, due to
 460 more vertically conductive flow, the homogeneous models tend to exhibit more apparent evaporation-
 461 driven expressions. However, while evaporation clearly impacts interface geometry to a de-
 462 gree, the extent to which evaporation controls interface dynamics when coupled with geologic
 463 heterogeneity and recharge requires further analysis.

464 These findings hold several implications for the future of numerically simulating density-
 465 dependent flow in arid and endorheic basins. Current density-dependent modeling of such basins
 466 typically produces simple representations of an aquifer, using homogeneous changes in anisotropy
 467 or simple layers with differing hydraulic conductivity values in order to shallow the interface
 468 geometry and match model results with observed field conditions. Considering that recharge
 469 may decrease in arid climates as a result of climate change, it is prudent to focus on the im-
 470 pacts of decreased inflow in the models (Wang et al., 2018). Modeling suggests that brine-to-
 471 freshwater interface migration distances are between 10-35% more sensitive to a decrease than
 472 an increase in inflow. These reactions highlight the importance of accounting for projected climate-
 473 driven changes in the hydrologic budgets of arid basins. Without considering the geologic com-

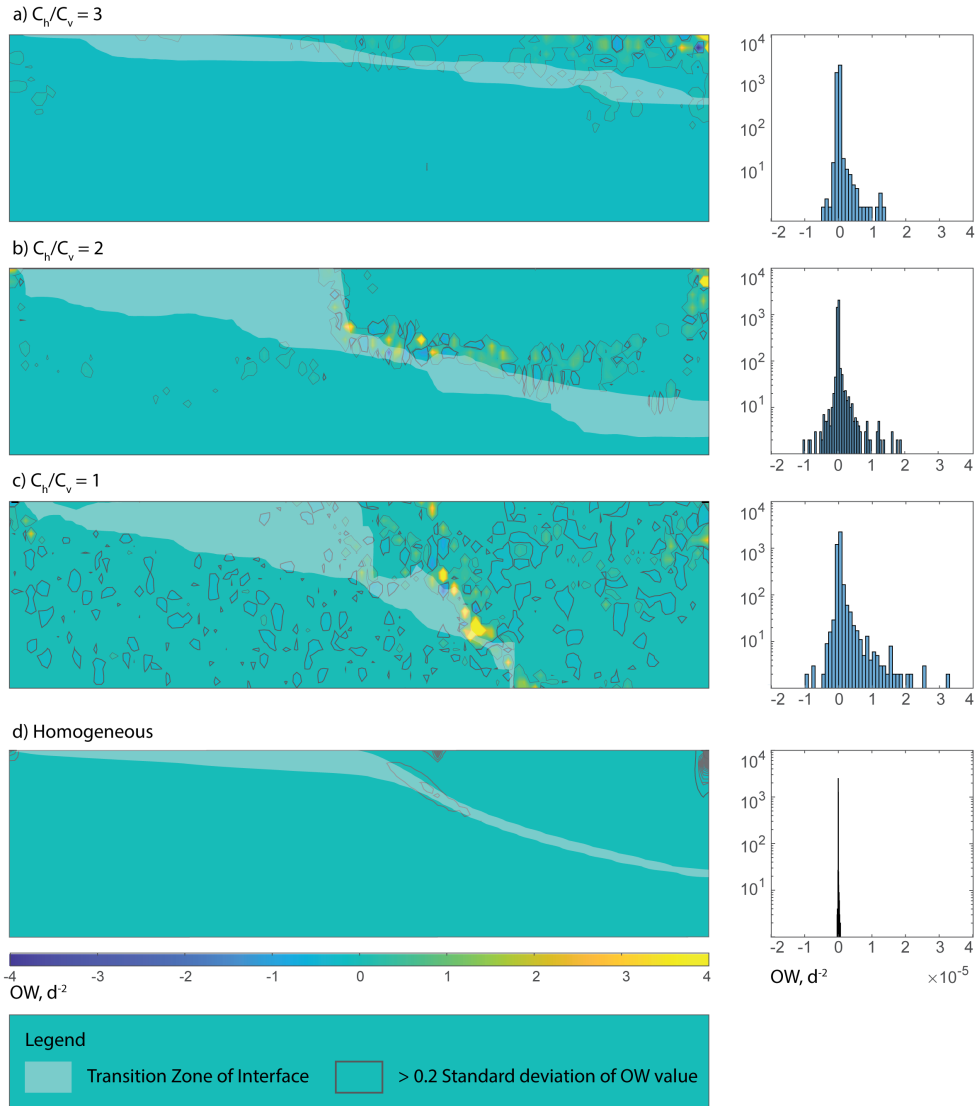


Figure 9. Spatial distributions and histograms of OW values for the same example simulations for each group from figure 5, with a) $c_h/c_v=3$, b) $c_h/c_v=2$, c) $c_h/c_v=1$, and d) homogeneous model. The white shaded areas indicate the physical location of the simulated interface's transition zone.

474 plexity or continuity of hydrostratigraphic units in an aquifer, such models result in conditions
 475 that may not produce either accurate geometries or reliable saline intrusion predictions. Thus
 476 homogeneous models are not suitable for understanding an aquifer's response to climate-driven
 477 changes in recharge. While simple changes in anisotropy may produce interface slopes that
 478 approach observed conditions, they do not account for local variation in the geometry, includ-
 479 ing the observed shallowing trend seen in the upper 50 meters of the aquifer of SdA. This sen-
 480 sitivity analysis documents that this shallowing trend impacts the density-driven response to
 481 changes in inflow. Accurate estimations of saline intrusion therefore require precise model-
 482 ing of geologic heterogeneity in order to more effectively assess geometry as well as response
 483 to changes in recharge and discharge mechanisms.

484 **5.4 Implications on future simulations of transient density-driven flow in brine-bearing** 485 **aquifers**

486 The majority of aquifers host a degree of subsurface heterogeneity regardless of depo-
 487 sitional environment. Results from this study elucidate the time-sensitivity of the interface's
 488 response to recharge which may be applicable to all brine-bearing aquifers. Coastal environ-
 489 ments have specific conditions that define the brine-to-freshwater interface and seawater cir-
 490 culation, but questions remain regarding the extent to which continuity in heterogeneity im-
 491 pacts the rates and distribution of subsurface groundwater discharge, especially in response to
 492 variations in recharge from inland aquifers (Russoniello et al., 2013). Horizontal hydrostrati-
 493 graphic continuity in heterogeneity addresses the question of geologic impact on interface sen-
 494 sitivity regardless of other physical characteristics that impact brine-bearing aquifers. Increased
 495 continuity in hydrostratigraphic units increases the time required for an interface to reach a new
 496 dynamic steady state by between 5 to 30 %. Longer, high-permeability conduits result in pref-
 497 erential pathways with localized hydraulic conditions that may differ from the effective hydraulic
 498 conductivity. These pathways create an unequal response in hydraulic head throughout an aquifer,
 499 which then leads to longer response times as differences in head require more time to stabi-
 500 lize throughout the flow field. This study thus suggests that continuity increases the timescales
 501 over which long-term variations in subsurface lateral recharge will manifest in saline ground-
 502 water intrusion, despite a range of other factors impacting brine-bearing aquifers such as coastal
 503 environments. Since high horizontal continuity is a common feature in depositional environ-
 504 ments, such as salt flats specifically, and arid, endorheic basins in general, homogeneous or
 505 simplistic modeling methods underestimate both the total amount of possible saline intrusion
 506 and the timescale at which migration can occur. This implies that predictions and analysis of
 507 transient saline intrusion in all brine-bearing aquifers must account for subsurface heterogene-
 508 ity, especially within interface-adjacent areas.

509 **5.5 Limitations of the simulation framework**

510 Randomized distributions of HK may not exactly represent the asymmetrical depositional
 511 environments of salt flats. Evaporite sequences produce geochemically zoned areas that of-
 512 ten abut facies with distinctly different hydrogeologic characteristics (Vásquez et al., 2013).
 513 This creates an asymmetric distribution of hydraulic conductivities, which randomized distri-
 514 butions of hydraulic conductivity may not accurately represent. Therefore, analysis of time con-
 515 stant values is limited to comparison among models. While a simple comparison with the HSF
 516 model indicates that most of the time constant values may seem plausible for playa environ-
 517 ments, the question of the realizations' geologic plausibility impedes the ability to rely on time
 518 constant values produced from these models as globally realistic scenarios.

519 Several hydrogeologic conditions remain homogeneous in the framework for the simu-
 520 lations, despite their direct correlation to changes in hydraulic conductivity. Specific yield, poros-
 521 ity, and anisotropy would be intrinsically heterogeneous, yet they remain consistently homo-
 522 geneous for computational simplicity given the number of realizations in the study's scope.
 523 Constant and homogeneous values for these variables may underrepresent the full impact of
 524 subsurface heterogeneity.

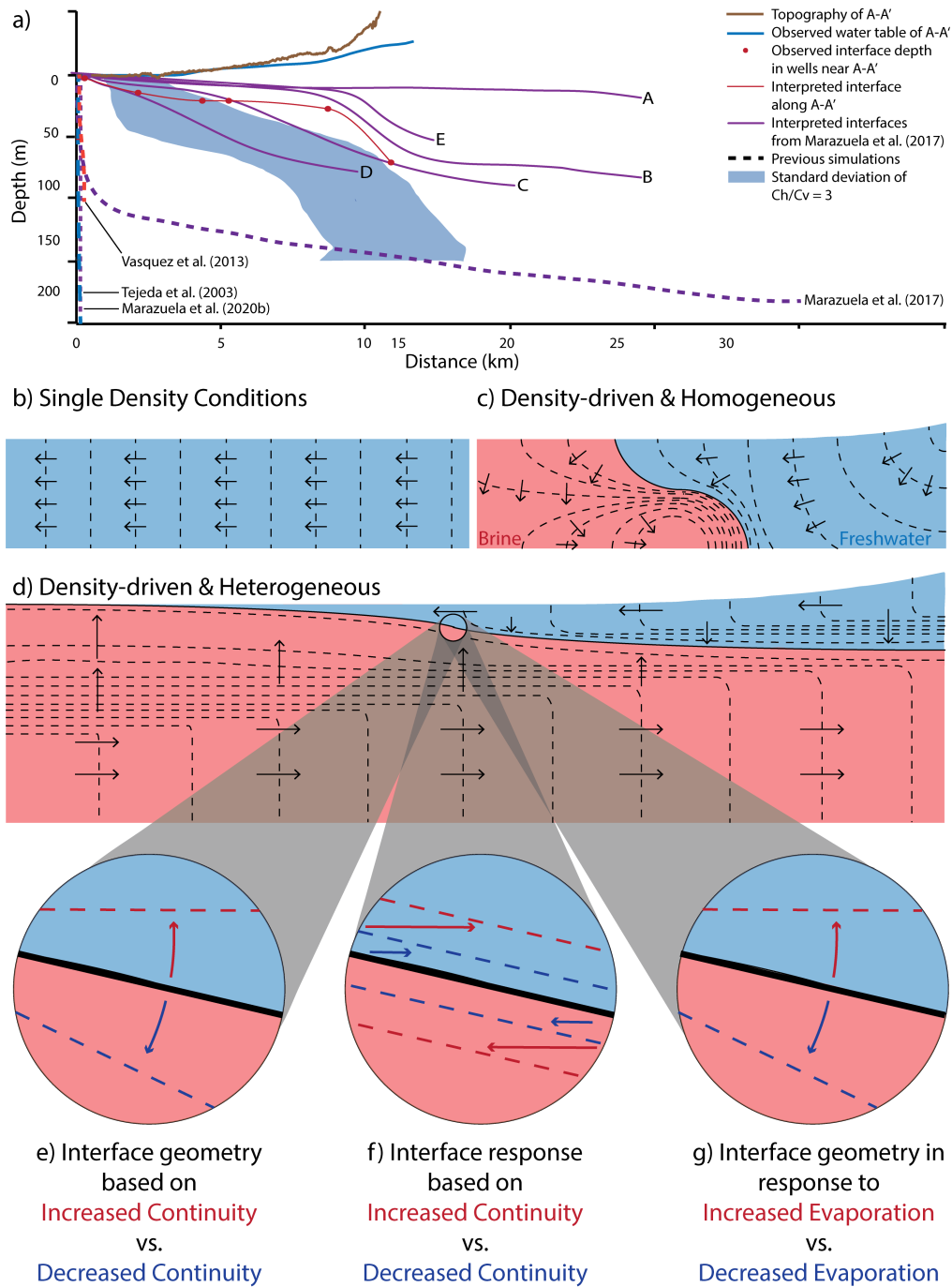


Figure 10. Conceptual illustration of results from observations of simulations with different distributions of hydraulic conductivity, with a) a comparison of this study’s simulations with previous studies, b) a homogeneous, single-density flow with black dashed lines showing potentiometric head contours, c) a homogeneous, variable-density flow model where the main determinant of interface geometry is the difference in density, and d) a heterogeneous model where the geometry of the interface is dependent on density and e) the extent of continuity in K . f) The sensitivity of the interface is also sensitive to continuity, g) The extent and rate of evaporation also has a likely impact on interface geometry.

6 Conclusion

Constraining the physical impacts of heterogeneity on the density-driven dynamics that control brine-to-freshwater interface migration and sensitivity is crucial for managing groundwater resources of brine-bearing aquifers in anticipation of climate-driven change. Homogeneous numerical simulations of density-driven flow fail to capture accurate geometry and presumably the dynamics of such interfaces. Aiming to develop a more accurate framework for the mechanisms driving density-driven fluid flow in arid basins, we assess the extent to which lateral hydrostratigraphic continuity impacts physical characteristics and time-sensitive behavior of the interface. To constrain the impact of continuity in geologic complexity, we employ a series of realizations of K with varying horizontal continuity. Following a perturbation in the simulated recharge to groundwater flow through each realization, we collect the interface slope, total distance that the interface travels, and the time required for the interface to reach a new steady-state in terms of an "e-folding" time constant.

The K distribution from the HSF of SdA produced a modeled interface that matched the observed location within 10 meters to a depth of 100 meters. Solute distribution results from the homogeneous counterpart of the HSF diverged from observed values. Simulated responses to perturbations in recharge from the HSF were also longer in both interface migration and migration response times than the homogeneous results. Results from the series of realizations of K distributions investigate whether the comparative observations can be attributed to hydrostratigraphic continuity in heterogeneity. Simulated values of concentration and hydraulic head best match observed conditions from SdA for the realizations with the strongest trend in horizontal continuity. Results further show a decrease in the slope of the interface as horizontal hydrostratigraphic continuity increases in the heterogeneous realizations, indicating that the improved matching of observed and simulated values is linked to the shallowing effect of increased continuity. This suggests that the relationship between the different hydrostratigraphic units and the resulting localized disequilibrium from those preferential pathways controls the distribution and sensitivity of hydraulic head. Our findings show a relationship between hydrostratigraphic continuity in heterogeneous environments and the resulting brine-to-freshwater interface response dynamics, with interface migration increasing by an order of magnitude and migration response times increasing by a factor of three when horizontal hydrostratigraphic continuity increases by a factor of two.

The results suggest that horizontal hydrostratigraphic continuity in heterogeneity impacts saline intrusion and therefore must be accounted for when modeling at all scales. The degree to which both anthropogenic extraction and ET coupled with hydrostratigraphic continuity impact interface dynamics remains undefined in arid basins. Future modeling initiatives using a similar geostatistical approach can address possible relationships on these different strains to brine-bearing aquifers. Arid regions throughout the world are experiencing strains on groundwater resources as anthropogenic exploitation and climate-driven aridity increases. This modeling approach constrains the density-driven dynamics of brine-to-freshwater interfaces in arid regions in response to climate-driven changes in recharge by establishing a first-order control between hydrostratigraphic continuity and density-driven dynamics. This study also confirms the importance of controlling time-sensitive reactions to changes in recharge for all brine-bearing aquifers.

7 Summary

Numerical simulations of density-driven groundwater flow along brine-to-freshwater interfaces that utilize equally probable representations of hydrostratigraphic heterogeneity indicate that geometry as well as the sensitivity and stability of interfaces depend on continuity of geologic units. While increased horizontal continuity leads to shallower and more anomalous expressions of the interface, increased continuity also results in higher sensitivity and more instability. Variable flow fields resulting from high hydraulic conductivity flow paths create an unstable environment in which the lack of connectivity prevents the most efficient reaction

576 in an aquifer in response to hydrologic changes. The results indicate that developing a hydros-
 577 tratigraphic conceptualization without identifying both the distribution of conductivity and the
 578 location of preferential flow risks the loss of accuracy in interpretations of density-driven fluid
 579 dynamics. These findings have implications for accurately assessing the risk of saline intru-
 580 sion and the sustainability of groundwater-fed shallow pool ecosystems in brine-bearing aquifers.

581 **Acknowledgments**

582 The authors would like to thank the Albemarle Corporation for supporting our ongoing research
 583 in order to further develop the understanding of density-driven flow dynamics. Special thanks
 584 to Jorge Garcia for his acumen and encouragement of our work. The data and model results
 585 presented may be obtained through the University of Massachusetts Data Repository. Fund-
 586 ing for this work was primarily provided by Albemarle Corporation and research on the sed-
 587 iment cores was supported by the National Science Foundation (grant number EAR1443226).

588 **References**

- 589 Bailey, R. (2015). Quantifying transient post-overwash aquifer recovery for atoll islands in
 590 the western pacific. *Hydrological Processes*, 29, 4470–4482.
- 591 Bear, J. (1972). Dynamics of fluids in porous media. *New York: Elsevier Science*, 53.
- 592 Boutt, D. F., Hynek, S., A, M. L., & G, C. C. (2016). Rapid recharge of fresh water to the
 593 halite-hosted brine aquifer of salar de atacama, chile. *Hydrological Processes*, 30,
 594 4720–4740.
- 595 Carle, S. (1999). T-progs: Transition probability geostatistical software. *University of Cali-
 596 fornia, Davis*, 1–78.
- 597 Carmona, V., Pueyo, J. J., Taberner, C., Chong, G., & Thirlwall, M. (2000). Solute inputs in
 598 the salar de atacama (n. chile). *Journal of Geochemical Exploration*, 69-70, 449–452.
- 599 Condon, L. E., & Maxwell, R. M. (2019). Simulating the sensitivity of evapotranspiration an
 600 streamflow to large-scale groundwater depletion. *Sci. Adv.*, 5, 1–9.
- 601 Corenthal, L., Boutt, D. F., Hynek, S., & Munk, L. A. (2016). Regional groundwater flow
 602 and accumulation of a massive evaporite deposit at the margin of the chilean altiplano.
 603 *Geophysical Research Letters*, 43(15), 8017–8025.
- 604 de Barros, F., Dentz, M., Koch, J., & Nowak, W. (2012). Flow topology and scalar mixing
 605 in spatially heterogeneous flow fields. *Geophysical Research Letters*, 39, 1–5. doi: 10
 606 .1029/2012GL051302
- 607 Duffy, J., & Hassan, S. (1988). Groundwater circulation in a closed desert basin: topo-
 608 graphic scaling and climatic forcing. *Water Resources Research*, 24(10), 1675–1688.
- 609 Eugster, H. P. (1980). Geochemistry of evaporitic lacustrine deposits. *Ann. Rev. Earth
 610 Planet. Sci.*, 8, 35–63.
- 611 Fan, Y., Duffy, C., & Oliver, D. (1996). Density-driven groundwater flow in closed desert
 612 basins : field investigations and numerical experiments. *Journal of Hydrology*, 196,
 613 139–184.
- 614 Ferguson, G., & Gleeson, T. (2012). Vulnerability of coastal aquifers to groundwater use and
 615 climate change. *Nature Climate Change*, 2, 342–345.
- 616 Gelhar, L. W., Welty, C., & Rehfeldt, K. R. (1992). A critical review of data on field-scale
 617 dispersin in aquifers. *Water Resources Research*, 28(7), 1955–1974.
- 618 Geng, X., & Boufadel, M. C. (2015). Impacts of evaporation on subsurface flow and salt ac-
 619 cumulation in a tidally influenced beach. *Water Resources Research*, 51, 5547–5565.
- 620 Geng, X., Boufadel, M. C., Rajaram, H., Cui, F., Lee, K., & An, C. (2020). Numerical study
 621 of solute transport in heterogeneous beach aquifers subjected to tides. *Water Resources
 622 Research*, 56, 1–20.
- 623 Haitjema, H. M., & Mitchell-Bruker, S. (2005). Are water tables a subdued replica of the to-
 624 pography? *Ground Water*, 43(6), 781–786.
- 625 Hamann, E., Kohfahl, C., Prommer, H., & Simmons, C. T. (2015). Numerical investigation
 626 of coupled density-driven flow and hydrogeochemical processes below playas. *Water*

- 627 *Resources Research*, 51, 9338–9352.
- 628 Heiss, J., Post, V., Laattoe, T., Russoniello, C., & Michael, H. (2017). Physical controls on
629 biogeochemical processes in intertidal zones of beach aquifers. *Water Resources Re-*
630 *search*, 53, 9225–9244. doi: 10.1002/2017WR021110
- 631 Heiss, J. W., & Michael, H. A. (2014). Saltwater-freshwater mixing dynamics in a sandy
632 beach aquifer over tidal, spring-neap, and seasonal cycles. *Water Resources Research*,
633 50, 6747–6766.
- 634 Hernández-López, M. F., Gironás, J., Braud, I., Suárez, F., & Muñoz, J. F. (2014). Assess-
635 ment of evaporation and water fluxes in a column of dry saline soil subject to different
636 water table levels. *Hydrological Processes*, 28, 3655–3669.
- 637 Houston, J. (2009). A recharge model for high altitude, arid, andean aquifers. *Hydrological*
638 *Processes*, 23, 2383–2393.
- 639 Houston, J., Butcher, A., Ehren, P., Evans, K., & Godfrey, L. (2011). The evaluation of brine
640 prospects and the requirement for modifications to filing standards. *Economic Geol-*
641 *ogy*, 106(7), 1125–1239.
- 642 Jordan, T. E., Mpodozis, C., Muñoz, N., Blanco, N., Pananont, P., & Gardeweg, M. (2004).
643 Cenozoic subsurface stratigraphy and structure of the salar de atacama basin, northern
644 chile. *Journal of South American Earth Sciences*, 122–146.
- 645 Jordan, T. E., Muñoz, N., Hein, M. C., Lowenstein, T., Godfrey, L., & Yu, J. (2002). Active
646 faulting and folding without topographic expression in an evaporite basin, chile. *Bul-*
647 *letin of the Geological Society of America*, 114(11), 1406–1421.
- 648 Ketabchi, H., Mahmoodzadeh, B., Ataie-Ashtiani, B., & Simmons, C. (2016). Sea-level rise
649 impacts on seawater intrusion in coastal aquifers: Review and integration. *Journal of*
650 *Hydrology*, 535, 235–255.
- 651 Klammler, H., Jawitz, J., Annable, M., Yaquain, J. A., Hatfield, K., & Burger, P. (2020).
652 Decadal scale recharge-discharge time lags from aquifer freshwater-saltwater interac-
653 tions. *Journal of Hydrology*, 582, 1–13. doi: 10.1016/j.jhydrol.2019.124514
- 654 Konikow, L. F., Akhavan, M., Langevin, C. D., Michael, H. A., & H, S. A. (2013). Seawater
655 circulation in sediments driven by interactions between seabed topography and fluid
656 density. *Water Resources Research*, 49(3), 1386–1399.
- 657 Kreyns, P., Geng, X., & Michael, H. A. (2020). The influence of connected heterogeneity on
658 groundwater flow and salinity distributions in coastal volcanic aquifers. *Journal of Hy-*
659 *drology*, 586, 1–10. doi: 10.1016/j.jhydrol.2020.124863
- 660 Kunasz, I. A. (1980). Lithium in brines. *Fifth Symposium on Salt*, 1, 115–117.
- 661 Langevin, C., & Guo, W. (2006). Modflow / mt3dms based simulation of variable-
662 density ground water flow and transport. *Ground Water*, 44(3), 339–351.
- 663 Liu, Y., Mao, X., Chen, J., & A, B. D. (2014). Influence of a coarse interlayer on seawater
664 intrusion and contaminant migration in coastal aquifers. *Hydrological Processes*, 28,
665 5162–5175.
- 666 Lowenstein, T. K., Hein, M. C., Bobst, A. L., Jordan, T. E., Ku, T. L., & Luo, S. (2003).
667 An assessment of stratigraphic completeness in climate-sensitive closed-basin lake
668 sediments: Salar de atacama, chile. *Journal of Sedimentary Research*, 73(1), 91–104.
- 669 Mahmoodzadeh, D., & Karamouz, M. (2019). Seawater intrusion in heterogeneous coastal
670 aquifers under flooding events. *Journal of Hydrology*, 568, 1118–1130. doi: 10.1016/
671 j.jhydrol.2018.11.012
- 672 Marazuela, M., Vázquez-Suñé, E., Custodio, E., Palma, T., Garcia-Gil, A., & Ayora, C.
673 (2018). Projections to the superior colliculus from inferior parietal, ventral premotor,
674 and ventrolateral prefrontal areas involved in controlling goal-directed hand actions in
675 the macaque. *Journal of Hydrology*, 561, 223–235.
- 676 Maxey, G. B. (1968). Hydrogeology of desert basins. *Groundwater*, 6(5), 10–22.
- 677 Meng, G., Han, Y., Wang, S., & Wang, Z. (2002). Seawater intrusion types and regional divi-
678 sions in the southern coast of laizhou bay. *Chinese Journal of Oceanology and Limnol-*
679 *ogy*, 20(3), 277–284.
- 680 Michael, H. A., & Khan, M. R. (2016). Impacts of physical and chemical aquifer hetero-
681 geneity on basin-scale solute transport: Vulnerability of deep groundwater to arsenic

- 682 contamination in bangladesh. *Advances in Water Resources*, 98, 147–158.
- 683 Michael, H. A., Scott, K. C., Koneshloo, M., Yu, X., Khan, M. R., & Li, K. (2016). Geo-
684 logic influence on groundwater salinity drives large seawater circulation through the
685 continental shelf. *Geophysical Research Letters*, 43(10), 782–791.
- 686 Montgomery, E. L., Rosko, M. J., Castro, S. O., Keller, B. R., & Bevacqua, P. S. (2003). In-
687 terbasin underflow between closed altiplano basins in chile. *Groundwater*, 41(4), 523–
688 531.
- 689 Morgan, L., Werner, A., & Simmons, C. (2012). On the interpretation of coastal aquifer wa-
690 ter level trends and water balances: A precautionary note. *Journal of Hydrology*, 280–
691 288.
- 692 Mpodozis, C., Arriagada, C., Basso, M., Roperch, C., & Reich, M. (2005). Late mesozoic
693 to paleogene stratigraphy of the salar de atacama basin, antofagasta, northern chile:
694 Implications for the tectonic evolution of the central andes. *Tectonophysics*, 399,
695 125–154.
- 696 Munk, L. A., Boutt, D. F., Hynek, S. A., & Moran, B. (2018). Hydrochemical fluxes
697 and processes contributing contributing to the formation of lithium-enriched
698 brines in a hyper-arid continental basin. *Chemical Geology*, 493, 37–57. doi:
699 10.1016/j.chemgeo.2018.05.013
- 700 Munk, L. A., Hynek, S. A., Bradley, D. A., Boutt, D. F., Labay, K., & Jochens, H. (2016).
701 Lithium brines: A global perspective. *Review in Economic Geology*, 18, 339–365.
- 702 Ortiz, C., Aravena, R., Briones, E., Suárez, R., Tore, C., & Muñoz, J. F. (2014). Sources of
703 surface water for the soncor ecosystem, salar de atacama basin, northern chile. *Hydro-
704 logical Sciences Journal*, 59(2), 336–350.
- 705 Philip, J. R., & van Duijn, C. J. (1996). Slumping of brine mounds: bounds on behaviour.
706 *Journal of Hydrology*, 179, 159–180.
- 707 Placzek, C., Quade, J., Betancourt, J. L., Patchett, P. J., Rech, J. A., Latorre, C., . . . English,
708 N. B. (2009). Climate in the dry central andes over geologic, millennial, and interannual
709 timescale. *Ann. Missouri Bot. Gard.*, 96(3), 386–397.
- 710 Post, V., Galvis, S. C., Sinclair, P. J., & Werner, A. D. (2019). Evaluation of management
711 scenarios for potable water supply using script-based numerical groundwater models
712 of a freshwater lens. *Journal of Hydrology*.
- 713 Post, V., Houben, J. G., & van Engelen, J. (2018). What is the ghjben-herzberg principle and
714 who formulated it? *Hydrogeology Journal*, 26(6), 1801–1807.
- 715 Post, V., Kooi, H., & Simmons, C. (2007). Using hydraulic head measurements in variable-
716 density ground water flow analyses. *Ground Water*, 45(6), 664–671.
- 717 Qureshi, A. S. (2011). Water management in the indus basin in pakistan: Challenges and op-
718 portunities. *Mountain Research and Development*, 31, 3.
- 719 Reutter, K. J., Charrier, R., Götze, H. J., Schurr, B., Wigger, P., Scheuber, E., . . . Belmonte-
720 Pool, A. (2006). The salar de atacama basin: a subsiding block within the western
721 edge of the altiplano-puna plateau. *Andes: Active Subduction Orogeny*, 303–325.
- 722 Rissman, C., Leybourne, M., Benn, C., & Christenson, B. (2015). The origin of solutes
723 within the groundwaters of a high andean aquifer. *Chemical Geology*, 396, 164–181.
- 724 Rosen, M. (1994). The importance of groundwater in playas: A review of playa classifica-
725 tions and the sedimentology and hydrology of playas. *Geological Society of America
726 Special Papers*, 289.
- 727 Russoniello, C. J., Fernandez, C., Bratton, J. F., Banaszak, J. F., Krantz, D. E., Andres, A. S.,
728 . . . Michael, H. A. (2013). Geologic effects on groundwater salinity and discharge
729 into an estuary. *Journal of Hydrology*, 498, 1–12.
- 730 Sanford, W. E., & Pope, J. P. (2010). Current challenges using models to forecast seawa-
731 ter intrusion: lessons from the eastern shore of virginia, usa. *Hydrogeology Journal*,
732 18(1), 73–93.
- 733 Sawyer, A., Lazareva, O., Kroeger, K. D., Crespo, K., Chan, C. S., Stieglitz, T., & Michael,
734 H. (2014). Stratigraphic controls on fluid and solute fluxes across the sediment-
735 water interface of an estuary. *Limnology and Oceanography*, 59, 997–1010. doi:
736 10.4319/lo.2014.59.3.0997

- 737 Scanlon, B. R., Keese, K. E., Flint, A. L., Flint, L. E., Gaye, C. B., Edmunds, W. M., &
738 Simmers, I. (2006). Global synthesis of groundwater recharge in semiarid and arid
739 regions. *Hydrological Processes*, *20*, 3335–3370.
- 740 Schaller, M. F., & Fan, Y. (2009). River basins as groundwater exporters and importers:
741 Implications for water cycle and climate modeling. *Journal of Geophysical Research*,
742 *114*, 1–20.
- 743 Schincariol, A., Schwartz, F., & Mendoza, C. (1997). Instabilities in variable density flows
744 : Stability and sensitivity analyses for homogeneous and heterogeneous media. *Water*
745 *Resources Research*, *33*, 31–41. doi: 10.1029/96WR02587
- 746 Stein, V., Yechieli, Y., Shalev, E., Kasher, R., & Sivan, O. (2019). The effect of pumping
747 saline groundwater for desalination on the fresh–saline water interface dynamics.
748 *Water Research*, *157*, 46–57.
- 749 Tejada, I., Cienfuegos, R., Muñoz, J. F., & Durán, M. (2003). Numerical modeling of saline
750 intrusion in salar de atacama. *Journal of Hydrologic Engineering*, *8*(1), 25–34.
- 751 Trabelsi, F., Ben Mammou, A., Tarhouni, J., Piga, C., & Ranieri, G. (2013). Delineation of
752 saltwater intrusion zones using the time domain electromagnetic method: The nabeul-
753 hammamet coastal aquifer case study. *Hydrological Processes*, *27*, 2004–2020.
- 754 Tyler, S. W., Muñoz, J. F., & Wood, W. W. (2006). The response of playa and sabkha hy-
755 draulics and mineralogy to climate forcing. *Groundwater*, *44*(3), 329–338.
- 756 Vásquez, C., Ortiz, P., Suárez, F., & Muñoz, J. (2013). Modeling flow and reactive transport
757 to explain mineral zoning in the atacama salt flat aquifer, chile. *Journal of Hydrology*,
758 *490*, 114–125.
- 759 Wang, J., Song, C., Reager, J., Yao, F., Famiglietti, J., Y, S., . . . Wada, Y. (2018). Recent
760 global decline in endorheic basin water storages. *Nature Geoscience*, *11*, 926–932.
- 761 Werner, A. D., Bakker, M., Post, V. E. A., Vandenbohede, A., Lu, C., Ataie-Ashtiani, B., . . .
762 Barry, D. A. (2013). Seawater intrusion processes, investigation and management:
763 Recent advances and future challenges. *Advances in Water Resources*, *51*, 3–26. doi:
764 10.1016/j.advwatres.2012.03.004
- 765 Werner, A. D., & Simmons, C. T. (2009). Impact of sea-level rise on sea water intrusion in
766 coastal aquifers. *Groundwater*, *47*(2), 197–204.
- 767 Wooding, R. A., Tyler, S. W., & White, I. (1997). Convection in groundwater below an
768 evaporating salt lake : 1 . onset of instability. *Water Resources Research*, *33*(6), 1199–
769 1217.
- 770 Yager, R., McCoy, K., Voss, C., E, S. W., & Winston, R. B. (2017). The role of uplift and
771 erosion in the persistence of saline groundwater in the shallow subsurface. *Geophys-
772 ical Research Letters*, *98*, 147–158.
- 773 Ye, M., Wang, L., Pohlmann, K. F., & Chapman, J. B. (2016). Evaluating groundwater inter-
774 basin flow using multiple models and multiple types of data. *Ground Water*, *54*(6), 1–
775 13.
- 776 Yechieli, Y. (2000). Fresh-saline ground water interface in the western dead sea area.
777 *Groundwater*, *38*(4), 615–623.
- 778 Yechieli, Y., Kafri, U., Goldman, M., & I, V. C. (2001). Factors controlling the configuration
779 of the fresh-saline water interface in the dead sea coastal aquifers: Synthesis of tдем
780 surveys and numerical groundwater modeling. *Hydrogeology Journal*, *9*(4), 367–377.
- 781 Yechieli, Y., Shalev, E., Kiro, Y., & Kafri, U. (2010). Response of the mediterranean and
782 dead sea coastal aquifers to sea level variations. *Water Resources Research*, *46*.
- 783 Yechieli, Y., & Wood, W. (2002). Hydrogeologic processes in saline systems: Playas,
784 sabkhas, and saline lakes. *Earth Science Reviews*, *58*, 343–365. doi: 10.1016/
785 S0012-8252(02)00067-3
- 786 Zhu, C., Waddell, R. K., Star, I., & Ostrander, M. (1998). Responses of ground water in
787 the black mesa basin, northeastern arizona, to paleoclimatic changes during the late
788 pleistocene and holocene. *Geology*, *26*(2), 127–130.